

The homogeneity scale in the Local Universe: model-independent estimate from S-PLUS DR4 blue galaxies

Camila Franco^{ID,*}, Felipe Avila^{ID,†}, Armando Bernui ^{ID,‡} and E. Telles

*Observatório Nacional, Rua General José Cristino, 77,
São Cristóvão, 20921-400, Rio de Janeiro, RJ, Brazil*

Ulisses Ribeiro and Clécio R. Bom ^{ID,§}

Centro Brasileiro de Pesquisas Físicas, Rua Dr. Xavier Sigaud 150, 22290-180 Rio de Janeiro, RJ, Brazil

Arianna Cortesi

*Instituto de Física, Universidade Federal do Rio de Janeiro, 21941-972, Rio de Janeiro, Brazil and
Observatório do Valongo, Ladeira Pedro Antonio, 43, 20080-090, Rio de Janeiro, Brazil*

W. Schoenell

*The Observatories of the Carnegie Institution for Science,
813 Santa Barbara St, Pasadena, CA 91101, USA*

T. Ribeiro

Rubin Observatory Project Office, 950 N. Cherry Ave., Tucson, AZ 85719, USA

A. Kanaan

*Departamento de Física,
Universidade Federal de Santa Catarina,
Florianópolis, SC, 88040-900, Brazil*

C. Mendes de Oliveira

Universidade de São Paulo, IAG, Rua do Matão 1225, São Paulo, SP, Brazil

(Dated: November 18, 2025)

We present a model-independent estimate of the angular homogeneity scale in the Local Universe by analysing data from the Southern Photometric Local Universe Survey (S-PLUS). Two complementary estimators are employed: (i) a parametric approach fitting the power-law of the two-point angular correlation function, which yields the homogeneity scale $\theta_H = 9.01^{+8.43}_{-3.61}$ deg; and (ii) a non-parametric fractal correlation dimension method, computing $D_2(\theta)$ directly from the correlation function, which results in $\theta_H = 6.28^{+8.72}_{-4.43}$ deg. From the mock catalogues generated with the GLASS algorithm, we find that the estimates from both methods are within 1σ of the median values obtained by applying both methodologies to the mocks. The transition scale to homogeneity, according to the Λ CDM model, is defined for matter, i.e. $b = 1$. Measurements of this scale with observational data clearly depends on the cosmic tracer analysed, and a calibration is necessary. Our study with blue galaxies, with bias $b \simeq 1$, provides a suitable estimate for comparison. Indeed, the results obtained in both approaches are compared with the value expected in the Λ CDM model, obtaining a good concordance.

Keywords: large-scale structure of Universe – cosmology: observations

I. INTRODUCTION

The cosmological principle (CP), one of the pillars of the standard cosmological model, postulates that on sufficiently large scales –and at any epoch– the universe should appear homogeneous and isotropic on average. Empirically, probing the validity of the CP with diverse cosmic tracers and at different epochs of the universe

evolution, is of paramount importance for the standard model, since it underpins the theoretical framework of the Λ CDM and its predictions for structure formation.

Isotropy has been extensively tested and confirmed using different tracers and cosmological observables (Bolejko & Wyithe 2009, Maartens 2011), such as quasars (Fujii 2022, Gonçalves et al. 2018b, Secrest et al. 2021), cosmic microwave background (CMB) (Aluri & Jain 2012, Kester et al. 2024, Khan & Saha 2022, Novaes et al. 2016, Planck Collaboration et al. 2020b), CMB lensing potential map (Marques et al. 2018), gravitational waves (Galloni et al. 2022), gamma-ray bursts (Bernui et al. 2008, Lopes et al. 2025, Rípa & Shafieloo 2019), galaxy clusters (Bengaly et al. 2017), galaxies (Appleby & Shafieloo 2014,

* camilafranco@on.br

† felipeavila@on.br

‡ bernui@on.br

§ debom@cbpf.br

Avila et al. 2019, Courtois et al. 2013, Gonçalves et al. 2018a, Sylos Labini & Baryshev 2010), and HI extragalactic sources (Avila et al. 2023, Franco et al. 2024, Wu & Xia 2025), between others. However, the homogeneity test presents observational challenges, especially when it comes to the use of photometric surveys, where the loss of radial information due to errors in redshift determination requires alternative approaches, such as purely angular analyses (Alonso et al. 2014).

Traditionally, some studies use counts on spheres (Scrimgeour et al. 2012) and on spherical caps (Laurent et al. 2016) to determine the transition scale to homogeneity, R_H and θ_H respectively, beyond which the distribution of matter tends asymptotically to the homogeneous regime. Studies on three-dimensional cosmic homogeneity have been carried out recently (Avila et al. 2022, Gonçalves et al. 2021, Ntelis et al. 2017); however, methods based on physical distances rely on cosmological assumptions to convert redshifts into distances, introducing potential biases (Clarkson 2012). One way to get around this issue is through model-independent analyses, which employ only angular coordinates (Alonso et al. 2014, Avila et al. 2018, 2019, Gonçalves et al. 2018a).

Thus, in this work we search for the angular scale of transition to cosmic homogeneity using photometric data from the Southern Photometric Local Universe Survey (S-PLUS). We will apply the scaled counts-in-caps estimator and the fractal correlation dimension to determine θ_H in a model-independent manner.

This work is organized as follows: Section II describes the observational data used in our analyses. In Section III, we outline the theoretical framework of the fractality. The log-normal simulations and the method to obtain it is presented in Section IV. The results are discussed in Section V. Finally, robustness tests are detailed in Section VI, and we summarize our conclusions in Section VII.

II. THE SOUTHERN PHOTOMETRIC LOCAL UNIVERSE SURVEY

The Southern Photometric Local Universe Survey (S-PLUS; Mendes de Oliveira et al. 2019) is an ongoing photometric survey designed to cover $\sim 9000 \text{ deg}^2$ across 12 filters using the T80-South telescope, located at the Cerro Tololo Observatory (Chile). The survey is in its public data release 4 (DR4), covering about 3000 deg^2 (Herpich et al. 2024).

The role of astrophysical parameters of red and blue galaxies, such as colour and luminosity, in the process of matter clustering is being studied and revealed (Croton et al. 2007, Mohammad et al. 2018, Ross et al. 2014, Zehavi et al. 2005). Blue galaxies are, in their majority, late-type galaxies with significant star formation, unlikely to be found in high-density regions (Dressler et al. 1997, Gerke et al. 2007), a feature that is reflected in clustering statistics as the two-point correlation function, where,

on small scales, red galaxies of any luminosity are more clustered than blue galaxies of any luminosity (Zehavi et al. 2005), meaning that blue galaxies exhibit weaker clustering features compared to red galaxies. In fact, blue galaxies are found in low-density regions where they exhibit reduced non-linear clustering effects, making the class of blue galaxies the suitable cosmic tracer for our analyses (Avila et al. 2024, Gerke et al. 2007, Mohammad et al. 2018, de Carvalho et al. 2021). Moreover, blue galaxies account for nearly 60% of galaxies in the Local Universe (Bamford et al. 2009), being, therefore, also more numerous in relation to red galaxies. For these reasons we follow the procedure described in Ribeiro et al. (2025) and select for our study a sample of blue galaxies from the S-PLUS DR4 (the color-color approach to select the blue galaxies sample follows the same criteria detailed explained in Ribeiro et al. (2025) and in Avila et al. (2019)).

We focus on a subsample within angular coordinates $150^\circ \leq \text{RA} \leq 165^\circ$ and $-48^\circ \leq \text{Dec} \leq -13^\circ$, that is, covering an area of $15^\circ \times 35^\circ = 525 \text{ deg}^2$, and in the redshift range $0 \leq z \leq 0.3$ (these are photometric redshifts, measured, processed, and derived by the S-PLUS team, released in the DR4 data). The selected sample contains 10,284 blue galaxies. The choice is driven because it is a contiguous completely observed sky patch, with suitable number density for the purposes of our analysis. The angular distribution of the full S-PLUS data and of the selected sample for analyses are shown in the upper and middle panels of Figure 1, while the lower panel presents the redshift distribution of the selected sample.

III. FRACTALITY AND HOMOGENEITY ESTIMATORS

The fractality concept plays an important role in analyses of cosmic structures distribution. A fractal ensemble is characterized by its fractal dimension, \mathcal{D} , which quantifies how the number of objects contained in a region of radius r scales with the size of this region. One expects that, at sufficiently large scales, an homogeneous and isotropic universe has a count number of objects proportional to the volume. On the other hand, at small scales, the distribution of galaxies exhibits fractal properties, reflecting the hierarchical structure of the cosmos (see, e.g., Alonso et al. (2014), Avila et al. (2018), Bagla et al. (2008), Coleman & Pietronero (1992), Ntelis et al. (2017), Pietronero (1987), Yadav et al. (2010) for more information about fractality).

In this study we do not assume a fiducial cosmology because we only use angular distances, in this sense our analyses provide model-independent estimates of the angular scale of homogeneity θ_H . In fact, we will analyse the data projected on the celestial sphere using the counts-in-spherical-caps estimator $N(<\theta)$. This function is defined as the mean number of points contained in a spherical cap of radius θ , centred in some point of reference. However,

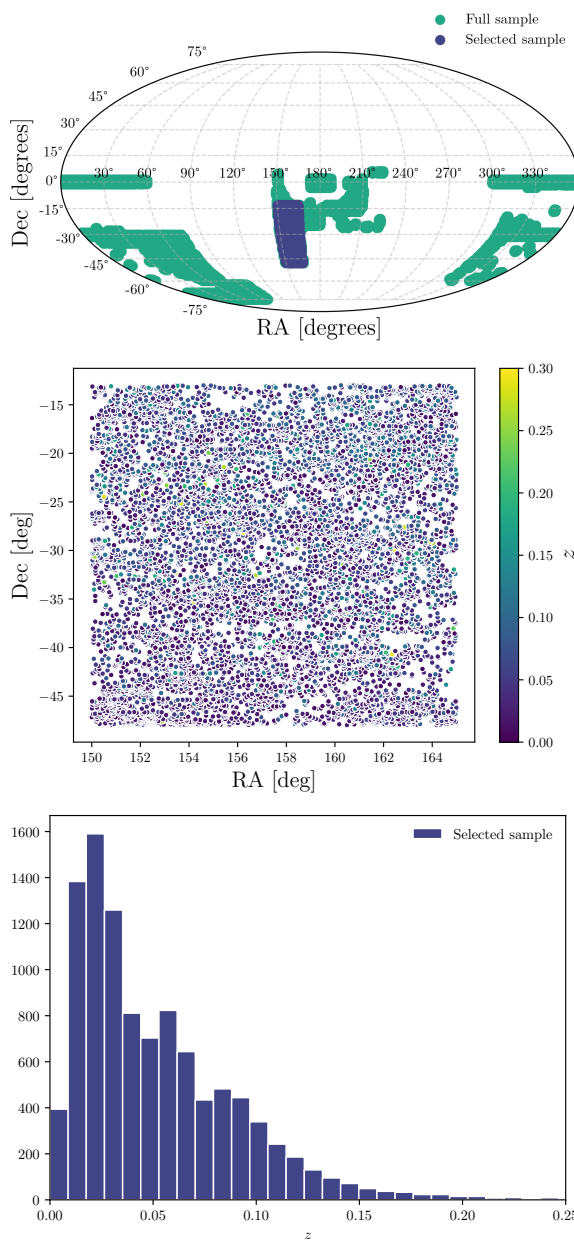


FIG. 1. Distribution of the S-PLUS blue galaxies corresponding to the public data release 4 (DR4). **Upper panel:** Sky coverage of the S-PLUS (green) and the selected sample (purple) in equatorial coordinates. **Middle panel:** Footprint of the selected sample. The colour scale represents the redshift range. **Bottom panel:** Redshift distribution of the selected sample.

due to the introduction of bias by the survey geometry, such as boundary effects, and possible observational incompleteness of the survey, it is not suitable to directly use $N(< \theta)$. Aiming to reduce these effects it is introduced the estimator scaled counts-in-spherical-caps, $\mathcal{N}(< \theta)$, originally defined as (Alonso et al. 2014, Scrimgeour et al.

2012)

$$\mathcal{N}(< \theta) \equiv \frac{N_{\text{gal}}(< \theta)}{N_{\text{rand}}(< \theta)}, \quad (1)$$

where $N_{\text{gal}}(< r)$ is the average counting estimated for spherical caps centred at each cosmic object of the data catalogue, and $N_{\text{rand}}(< r)$ is the same quantity calculated upon a random homogeneous sample, using as centres the coordinate positions of the data catalogue sources. Notice that the random catalogue has the same geometry and completeness of the observational data, but with a significant higher density; for our analyses, we constructed a random catalogue 10 times denser than the sample of blue galaxies in study.

The fractal dimension for data projected on the celestial sphere is defined as (Gonçalves et al. 2018a)

$$\mathcal{D}_2(\theta) \equiv \frac{d \ln \mathcal{N}(< \theta)}{d \ln \theta} + \frac{\theta \sin \theta}{1 - \cos \theta}. \quad (2)$$

Note that the angular scale of homogeneity, θ_H , is obtained when $\mathcal{D}_2(\theta) \rightarrow \theta \sin \theta / (1 - \cos \theta)$. More precisely, one finds θ_H by adopting the 1% criterion described by Scrimgeour et al. (2012). According to this, the homogeneity scale is reached when the fractal dimension \mathcal{D}_2 attains at $\theta = \theta_H$ the 99% of its limiting value

$$\mathcal{D}_2(\theta_H) = 0.99 \left[\frac{\theta \sin \theta}{1 - \cos \theta} \right]_{\theta=\theta_H}. \quad (3)$$

This criterion, first defined in Scrimgeour et al. (2012), proved to be the most suitable. In fact, simulations constructed with a specific homogeneity scale were analysed, and such scale was recovered with the best accuracy using this criterion. In addition, it has an interesting feature of being survey-independent, enabling it to be used in comparisons across different measurements and cosmological models.

A. Landy-Szalay methodology

In this section we present the first approach, termed the LS methodology, to find θ_H . This approach uses the two-point angular correlation function (TPACF), $\omega(\theta)$, to define the scaled counts-in-caps $\mathcal{N}(< \theta)$. For this scope, we adopt the Landy-Szalay (LS) estimator (Landy & Szalay 1993)

$$\omega(\theta) = \frac{DD(\theta) - 2DR(\theta) + RR(\theta)}{RR(\theta)}, \quad (4)$$

where $DD(\theta)$ is the number of data-data pairs, $RR(\theta)$ is the number of random-random pairs, and $DR(\theta)$ is the number of data-random pairs, all within an angular bin centred at θ . These quantities are normalized by the total

number of possible pairs in each case, that is

$$DD(\theta) = \frac{2 dd(\theta)}{n_g(n_g - 1)}, \quad (5)$$

$$RR(\theta) = \frac{2 rr(\theta)}{n_r(n_r - 1)}, \quad (6)$$

$$DR(\theta) = \frac{dr(\theta)}{n_g n_r}, \quad (7)$$

with n_g (n_r) being the number of galaxies in the data (random) catalogue, and $dd(\theta)$, $rr(\theta)$, $dr(\theta)$ are the raw pair-counts of each case. This normalization accounts for the different sample sizes of the data and random catalogues.

Then, $\mathcal{N}(< \theta)$ is defined considering the cumulative scaled counts-in-caps (Alonso et al. 2014, Avila et al. 2018)

$$\mathcal{N}(< \theta) \equiv 1 + \bar{\omega}(\theta), \quad (8)$$

where

$$\bar{\omega}(\theta) \equiv \frac{1}{1 - \cos \theta} \int_0^\theta \omega(\theta') \sin \theta' d\theta', \quad (9)$$

is the average angular correlation function for a given spherical cap with angular size θ .

After calculating the TPACF given by equation (4), we fit the TPACF by a power-law function

$$\omega(\theta) = \left(\frac{\theta}{\theta_0} \right)^{-\beta}, \quad (10)$$

where the parameters θ_0 and β are related to the transition scale between linear and non-linear regimes, and the slope of the correlation, respectively (Coil 2013a,b, Connolly et al. 2002, Franco et al. 2025a, Kurki-Suonio 2023, Marques & Bernui 2020, Peebles 1993, Totsuji & Kihara 1969). Then we compute $\mathcal{N}(< \theta)$ using equation (8), and $\mathcal{D}_2(\theta)$ using equation (2).

For this analysis, we compute the TPACF by applying 15 logarithmically spaced bins within the angular range $[\theta_{\min}, \theta_{\max}] = [0.05^\circ, 7^\circ]$, as can be seen in Figure 2. This interval was chosen to best capture the power-law behaviour of the TPACF. The parameters θ_0 and β are determined by fitting equation (10) using the CURVEFIT¹ (Virtanen et al. 2020) package. Then, we use equation (2) to calculate the correlation dimension $\mathcal{D}_2(\theta)$ by computing the logarithmic derivative of equation (8), where $\mathcal{N}(\theta)$ itself is constructed using the fitted power-law form of equation (10).

B. Angular fractal correlation dimension

In this section we present the second approach, termed the angular fractal correlation dimension (AFCD) methodology, to find θ_H . The study of the angular scale of homogeneity has the advantage of eliminating the necessity to adopt a fiducial model to convert redshifts into cosmological distances. That way, the two-dimensional version of the fractal dimension, $\mathcal{D}_2(\theta)$, is obtained through considerations analogous to the three-dimensional case, substituting spheres by spherical caps in the sky.

Using the definition of equation (8), equation (2) becomes

$$\mathcal{D}_2(\theta) = \frac{\theta}{1 + \bar{\omega}(\theta)} \frac{d\bar{\omega}(\theta)}{d\theta} + \frac{\theta \sin \theta}{1 - \cos \theta}. \quad (11)$$

Taking the derivative of equation (9) with respect to θ , including it in equation (11), and simplifying terms, one obtains (details of the deduction of this equation are presented in Appendix A)

$$\mathcal{D}_2(\theta) = \frac{\theta \sin \theta}{1 - \cos \theta} \left[\frac{1 + \omega(\theta)}{1 + \bar{\omega}(\theta)} \right]. \quad (12)$$

To compute the TPACF, we used the public code TREECORR² (Jarvis 2015), applying 20 logarithmically spaced bins within the angular range $[\theta_{\min}, \theta_{\max}] = [0.05^\circ, 40^\circ]$. A random catalogue was constructed, maintaining the same angular footprint as the original region but with a uniform distribution of points and a number density 10 times greater than that of the observed dataset.

IV. GLASS SIMULATIONS

In our analyses we use mock realizations produced by the GLASS (Generator for Large Scale Structure; Tessa et al. (2023))³ numerical code. Codes that generate log-normal simulations can realistically reproduce the statistical properties of large observational surveys and their covariance matrix (Blot et al. 2019, Colavincenzo et al. 2019, Lippich et al. 2019). The GLASS code is particularly well-suited for this work. It achieves these objectives by generating matter density fields in a series of spherical shells nested around the observer, effectively discretizing the past light cone, from the present day up to high redshift. GLASS uses the linear matter power spectrum from a given fiducial cosmology as its primary input to generate the matter density fields. This method allows for the efficient production of a large number of mock realizations that accurately capture the two-point statistics. A key feature of GLASS is its use of a log-normal model

¹ https://docs.scipy.org/doc/scipy/reference/generated/scipy.optimize.curve_fit.html

² https://rmjarvis.github.io/TreeCorr/_build/html/index.html

³ <https://glass.readthedocs.io/stable/index.html>

to translate the initial Gaussian density field into a more realistic, non-linear distribution of matter.

The simulation setup defines the comoving radial resolution or redshift grid, z_{grid} , the choice of radial window function, $W(z)$, the number of correlated redshift shells, n_c , the galaxy bias, b , the mask resolution, n_{side} , and the maximum multipole, l_{max} employed to evaluate the angular power spectrum, and the photometric redshift error σ_0 at $z = 0$. To accurately reproduce the properties of our data, the code takes as input both the survey mask, and the distribution of galaxies per redshift interval and per square degree. Table I lists the set of input values used for generating the 1,000 log-normal mock catalogues for our analyses.

TABLE I. Survey configuration and cosmological parameters used to generate the set of 1,000 mock catalogues. We use a top-hat window function.

Survey configuration	Cosmological parameters
$z_{\text{grid}} = [0.0 - 0.3, 0.05]$	$\Omega_c h^2 = 0.1202$
$n_c = 6$	$\Sigma m_\nu = 0.06 \text{ eV}$
$b = 1.0$	$n_s = 0.9649$
$n_{\text{side}} = 2048$	$\ln(10^{10} A_s) = 3.045$
$l_{\text{max}} = 2048$	$\Omega_b h^2 = 0.02236$
$\sigma_0 = 0.03$	$h = 0.67021$

V. RESULTS

In this section, we present the main results of our analyses regarding the estimation of the angular scale of homogeneity from clustering measurements, results obtained applying the two methodologies described above namely, the analysis using the LS and AFCD methodologies.

A. Results with the LS methodology

Our first analyses are done with the Landy-Szalay estimator, described in Section III A. For this, we calculated the TPACF for our data sample within the angular interval $[0.05^\circ, 7^\circ]$, as presented in Figure 2. The blue markers are obtained from the data, while the ensemble of gray lines shows 1,000 mock realizations generated with the same sample geometry. The power-law trend is well captured by the fitting of equation (10), outlined in the red, continuous line. Note that, even at the smallest angles, the GLASS simulations reproduce the observed clustering amplitude, indicating that our mocks are suitable reproductions of the data.

The measured $\mathcal{D}_2(\theta)$ over the range $\theta \in [1^\circ, 20^\circ]$ is presented in Figure 3. Applying the 1% criterion of equation (3), we find the angular scale of homogeneity

$$\theta_H = 9.01^{+8.43}_{-3.61} \text{ deg}, \quad (13)$$

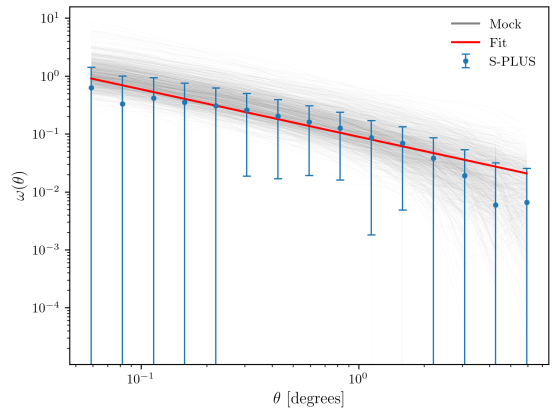


FIG. 2. The TPACF, $\omega(\theta)$, calculated from the blue galaxies sample following the Landy-Szalay methodology (see Section III A for details). The blue dots represent the binned TPACF data with 1σ uncertainties, and the gray curves are the TPACF computed for each one of the mocks. The solid red line corresponds to the best-fit model (see equation (10)).

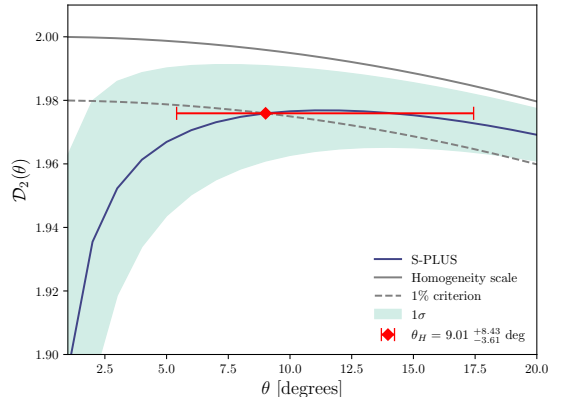


FIG. 3. The correlation dimension, $\mathcal{D}_2(\theta)$, for the LS methodology. The solid blue curve was obtained from equation (2), with the shaded region representing the 1σ interval. The solid gray line marks the theoretical expectation for a perfectly homogeneous angular distribution, while the dashed gray line corresponds to the 1% criterion. The red mark indicated the angular homogeneity scale, $\theta_H = 9.01^{+8.43}_{-3.61} \text{ deg}$, defined as the transition where the measured $\mathcal{D}_2(\theta)$ meets the criterion.

as summarized in Table II.

To assess the statistical robustness, we measured θ_H in 1,000 mocks generated with GLASS. Figure 4 displays the distribution of the values across these mocks.

The vertical green line corresponds to the median value, $\tilde{\theta}_H = 8.52 \text{ deg}$ for the set of 1,000 mocks, and the green shaded region is the 1σ interval. Therefore, the deviation is within the 1σ confidence interval.

TABLE II. Angular scale of transition to homogeneity, θ_H , and the respective Λ CDM predictions, for both methodologies.

	LS estimator			AFCD estimator		
	Data	Mocks	Λ CDM	Data	Mocks	Λ CDM
θ_H	$9.01^{+8.43}_{-3.61}$ deg	8.52 deg	8.14 deg	$6.28^{+8.72}_{-4.43}$ deg	9.83 deg	8.09 deg

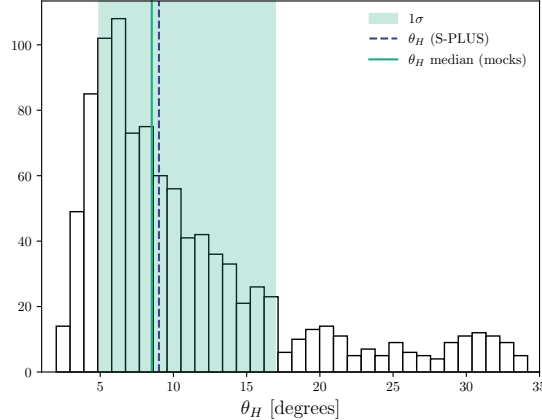


FIG. 4. Distribution of angular homogeneity scales measured from 1,000 mock catalogues using the LS methodology. The green vertical line indicates the median $\theta_H = 8.52$ deg, obtained from the mocks, while the green shaded region corresponds to the 1σ confidence interval. The blue dashed line corresponds to the value obtained analysing the S-PLUS blue galaxies sample, that is, $\theta_H = 9.01$ deg (see Table II).

B. Results with AFCD methodology

As presented in Section III B, the results obtained via equation (12) differs from the previous one in that it employs a more direct approach, without the need to fit a power-law model, and that relies exclusively on the profile of $\omega(\theta)$. Therefore, $\mathcal{D}_2(\theta)$ is calculated directly from the data, being a valid approximation of the classical counts-in-caps method.

We employ this approach by computing $\omega(\theta)$ on 20 logarithmically spaced bins in $\theta \in [0.05^\circ, 40^\circ]$ (see Figure 5) and evaluating the correlation dimension using equation (12). Figure 6 shows the resulting $\mathcal{D}_2(\theta)$.

Applying the 1% criterion of equation (3), we found that the resulting angular scale is

$$\theta_H = 6.28^{+8.72}_{-4.43} \text{ deg.} \quad (14)$$

The histogram of $\{\theta_H\}$ values obtained from the mocks is shown in Figure 7. The deviation from the mocks median $\tilde{\theta}_H = 9.83$ deg value is also within 1σ CL.

The non-parametric AFCD approach differs from the previous one in the way how the fractal dimension, $\mathcal{D}_2(\theta)$, is calculated. In the parametric approach, $\mathcal{D}_2(\theta)$ is derived from $\mathcal{N}(< \theta)$, which reduces the impact of statistical fluctuations at large angular scales. However, this attenuation feature tends to shift the transition scale to slightly larger

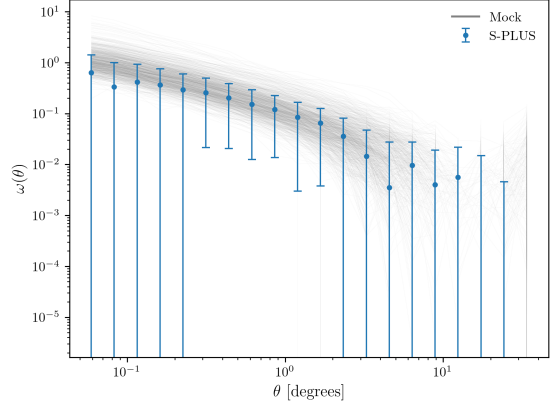


FIG. 5. Same as Figure 2, but for the Angular Fraction Correlation Dimension methodology (see Section III B for details). Note that we did not fit the data because this approach does not use the best-fit parameters of the TPACF.

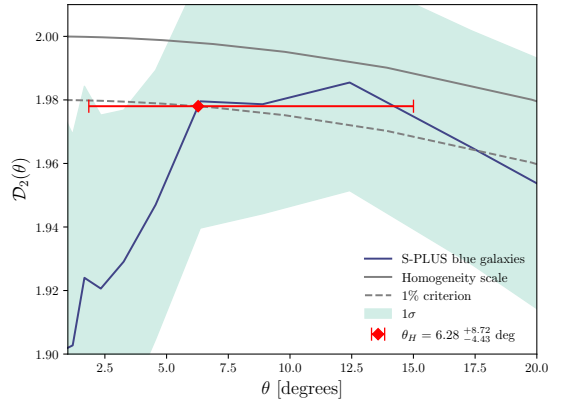


FIG. 6. Same as Figure 3, but for the AFCD methodology using equation (12). The homogeneity scale, in this case, corresponds to $\theta_H = 6.28^{+8.72}_{-4.43}$ deg.

angles. In contrast, the non-parametric approach, instead of deriving $\mathcal{N}(< \theta)$, directly applies equation (12), which avoids numerical differentiation of the correlation function. This is particularly advantageous, since numerical derivatives are more sensitive to statistical noise, binning effects in the TPACF, and rounding errors than numerical integration. As a consequence, the method reduces the impact of statistical fluctuations at large angular scales, though it tends to anticipate the transition when small fluctuations push $\mathcal{D}_2(\theta)$ to the threshold value.

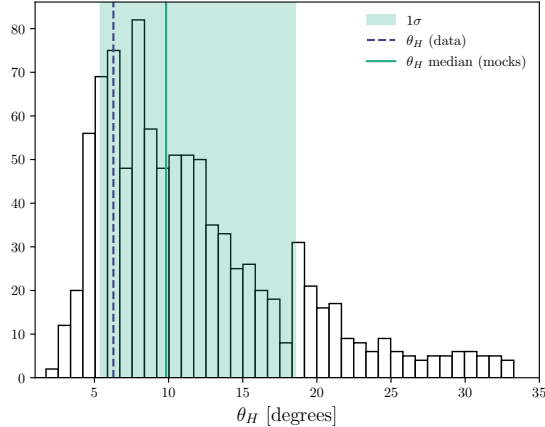


FIG. 7. Same as Figure 4, but for the AFCD methodology using the equation (12). The median value corresponds to $\theta_H = 9.83$ deg.

C. Theoretical prediction of θ_H

To quantify the theoretical expectation of the angular transition to cosmic homogeneity, we compute the TPACF predicted by the flat- Λ CDM cosmology. This quantity encapsulates, in projection, the statistical imprint of the three-dimensional matter distribution on the celestial sphere, and is given by the double integral over the redshift (Crocce et al. 2011),

$$\omega_{\text{th}}(\theta) = \int_0^\infty dz_1 \phi(z_1) \int_0^\infty dz_2 \phi(z_2) \xi(s), \quad (15)$$

where $\xi(s)$ is the spatial two-point correlation function evaluated at the comoving separation s and $\phi(z)$ is the normalized selection function describing the redshift distribution of galaxies, $n(z)$, as

$$\phi(z) = \frac{n(z)}{\int n(z) dz}. \quad (16)$$

Given two cosmic objects at redshifts z_1 and z_2 , respectively, separated by an angle θ , the comoving separation considering a Friedmann-Lemaître-Robertson-Walker (FLRW) metric is

$$s = \sqrt{\chi^2(z_1) + \chi^2(z_2) - 2\chi(z_1)\chi(z_2)\cos\theta}, \quad (17)$$

where $\chi(z)$ is the comoving radial distance

$$\chi(z) = \frac{c}{H_0} \int_0^z \frac{dz'}{\sqrt{\Omega_m(1+z)^3 + \Omega_\Lambda}}, \quad (18)$$

for the flat- Λ CDM model, which we calculate using the Cosmic Cosmology Library⁴ (CCL; Chisari et al. 2019).

⁴ <https://github.com/LSSTDESC/CCL>

The spatial two-point correlation function is related to the matter power-spectrum, $P(k, z)$, through the Fourier transform

$$\xi(s, z) = \int_0^\infty \frac{dk}{2\pi^2} k^2 j_0(ks) P(k, z), \quad (19)$$

where j_0 is the spherical Bessel function of the first kind of order zero.

To compute $P(k, z)$, we use the CAMB⁵ code (Lewis & Challinor 2011), adopting a flat- Λ CDM cosmology with parameters consistent with the last Planck Collaboration et al. (2020a), as summarized in Table I.

After obtaining the theoretical correlation function, we applied the same methodologies described in Sections III A and III B to determine the theoretical angular scale of transition to homogeneity. The resulting values are $\theta_H^{\Lambda\text{CDM}} = 8.14$ deg for the LS method and $\theta_H^{\Lambda\text{CDM}} = 8.09$ deg for the AFCD method. These estimates are summarized in Table II, alongside the observational measurements obtained from the data. Considering the mean uncertainty of the observational results, $\bar{\sigma} = (\sigma_+ + \sigma_-)/2$, our estimates using the LS and AFCD methods are 0.14σ and 0.28σ away from the Λ CDM expectation, respectively. This means that our results from both approaches are consistent one to the other, and in good agreement with the scales provided by the standard cosmological model Λ CDM.

VI. ROBUSTNESS TESTS VIA RESAMPLING

Photometric uncertainties can significantly impact tomographic analyses, altering the number of galaxy pairs within a given redshift slice and, thereby, biasing the inferred angular correlation function. To mitigate these effects and to ensure the reliability of our results, we implement a resampling technique (Asorey et al. 2016, Ribeiro et al. 2025) based on the individual redshift probability distribution function (PDF) provided for each galaxy in the S-PLUS catalogue. Each PDF, $p_i(z)$, is modelled as a weighted sum of Gaussian components,

$$p_i(z) = \sum_k w_{ik} \mathcal{N}(z|\mu_{ik}, \sigma_{ik}), \quad (20)$$

where w_{ik} , μ_{ik} , and σ_{ik} denote the weight, mean and standard deviation of the k -th Gaussian component, respectively. These parameters capture the multimodal and asymmetric structure of photometric redshift estimates (Herpich et al. 2024)⁶.

⁵ <https://camb.info/>

⁶ For more information about the columns in the data catalogue, see, for example, https://datalab.noirlab.edu/data-explorer?showTable=splus_dr4.photoz and <https://www.splus.cloud/documentation/DR4> and the references therein.

We employ the inverse transform sampling method to generate realizations of the galaxy distribution consistent with these PDFs. For each galaxy i , we first construct its normalized PDF on a redshift grid $z \in [0, 1]$ with 10,000 sampling points. The cumulative distribution function

$$C_i(z) = \int_{z_{min}}^{z_{max}} p_i(z') dz', \quad (21)$$

is then computed. Random values $u_j \in [0, 1]$ are drawn from a uniform distribution, and the corresponding sampled redshifts are obtained as $z_{ij} = C_i^{-1}(u_j)$, with i and j denoting the i -th galaxy and the j -th resampling realization, respectively. This procedure is repeated for all galaxies to produce one complete realization of the dataset. Repeating the process $N_d = 1,000$ times yields a set of resampled catalogues, each representing a statistically consistent dataset of the observed data driven by the photometric-redshift uncertainties.

Each realization is then subject to the same tomographic selection used in the analysis. Specifically, galaxies are assigned to redshift slices of width Δz , chosen to be larger than the typical redshift uncertainty, $\langle \sigma_z \rangle$, in order to minimize boundary effects. In this way, the analysis slice covers $z \in [0, 0.3]$, while the PDFs are defined on a broader grid $z \in [0, 1]$, ensuring that the tails of the distributions are fully represented. In this sense, galaxies whose PDFs partially overlap the tomographic boundaries can contribute to multiple realizations, thus preserving the statistical information encoded in the photo- z uncertainties. Figure 8 illustrates the resampling method for a subset of galaxies.

The ensemble of $N_d = 1,000$ resampled catalogues produced an equal number of TPACF measurements that are statistically consistent with each other, exhibiting only a small dispersion around the mean correlation function, as can be seen in Figure 9. The modest spread can be directly attributed to the combination of a relatively broad tomographic bin, i.e. $z \in [0, 0.3]$ and the narrowness of the individual photo- z PDFs. Because the vast majority of galaxies have $p_i(z)$ sharply peaked well inside the adopted interval, their inclusion or exclusion in any given realization is virtually unchanged. Consequently, the effective angular footprint of the sample remains stable and the TPACF, being purely angular, shows minimal sensitivity to the perturbations in z .

This outcome can be interpreted as follows: the measured clustering signal is robust against uncertainties in z , and the resampling analysis confirms that the angular correlation measurements can be safely used. It is worth noting, however, that the features observed in this resampling is specific to the chosen redshift interval. For narrower tomographic bins or broader $p(z)$ distributions, the same procedure would yield noticeably larger dispersion, as more galaxies would cross the bin boundaries between realizations (see, for example, Ribeiro et al. (2025)).

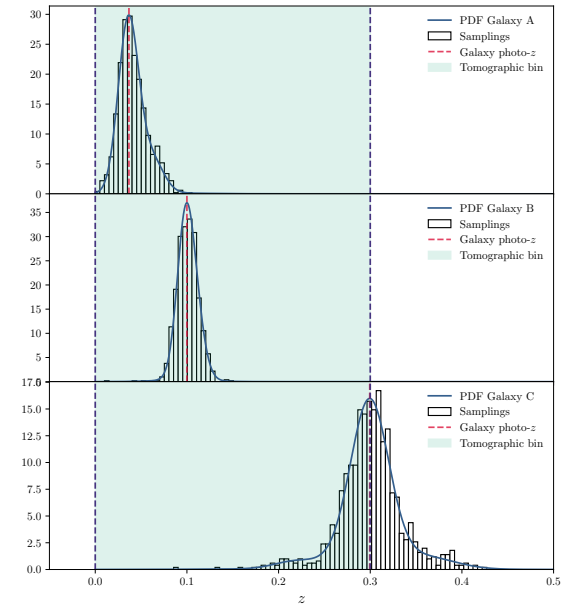


FIG. 8. Sampling of galaxies. For each galaxy, the solid curve represents its reconstructed redshift PDF, $p(z)$, while the histogram shows the distribution of 10,000 redshift draws obtained through random resampling of the Gaussian mixture components using the weights. The vertical dashed line marks the catalogue photometric redshift, and the shaded region corresponds to the tomographic slice adopted in the analysis.

VII. CONCLUSIONS

The observed universe is highly inhomogeneous, in particular in the Local Universe, with huge matter structures and large voids distributed everywhere (Courtois et al. 2013, 2025, Einasto 1991, Franco et al. 2025b, Gavas et al. 2025, Novaes et al. 2025, Telles & Maddox 2000). On the other hand, inhomogeneities were tiny in the distant past, as revealed by the CMB temperature fluctuations, therefore there was a cosmic evolution from homogeneously distributed density fluctuations to a clumpy inhomogeneous universe (Huterer 2023, Marques & Bernui 2020). This leads to the natural question regarding a minimum scale, at any epoch, from which one can consider the matter content in the universe as homogeneously distributed (Alonso et al. 2014, Avila et al. 2022).

Thus, in this work, we presented a model-independent estimate of the angular homogeneity scale in the Local Universe using 10,284 blue galaxies within the redshift range $0 \leq z < 0.3$ from the S-PLUS catalogue. We applied two complementary estimators – a parametric power-law fit to the TPACF and a non-parametric fractal correlation dimension analysis – obtaining consistent results for the homogeneity scale, with $\theta_H = 9.01^{+8.43}_{-3.61}$ deg and $\theta_H = 6.28^{+8.72}_{-4.43}$ deg, respectively. Some words are in due regarding the differences observed in the fractal dimension function $\mathcal{D}_2(\theta)$ shown in figures 3 and 6. In fact, while the LS methodology smooths the TPACF through the

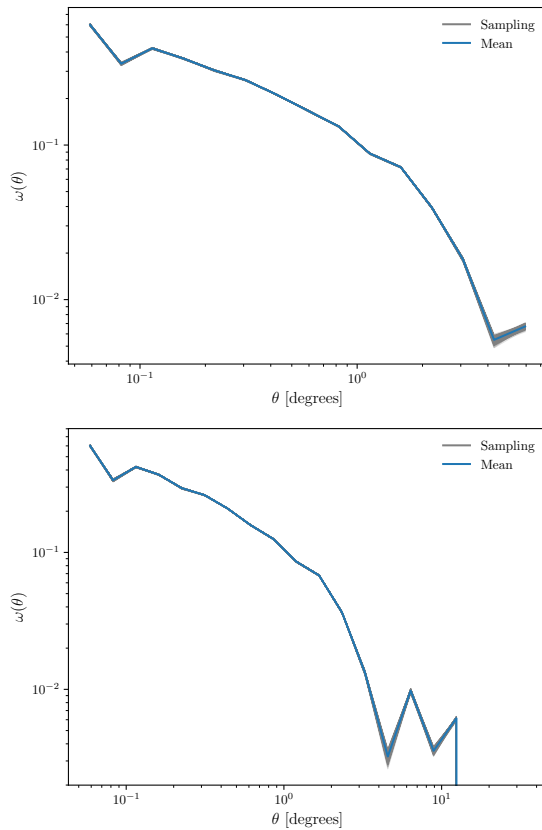


FIG. 9. The TPACF computed for the set of 1,000 resampled catalogues. The gray lines correspond to the TPACF for each individual sampling, while the blue line denotes their mean. The horizontal axes match those of Figures 2 and 5, respectively, shown in Section V. **Upper panel:** Analyses done on the resampled catalogues using the LS methodology. **Bottom panel:** Analyses done on the resampled catalogues using the AFCD methodology.

power-law given in equation (10), the AFCD approach uses the angular correlation function $\omega(\theta)$ computed from the S-PLUS catalogue, where clusters of galaxies and large voids are present (making the TPACF noisy). The difference in the way $\mathcal{D}_2(\theta)$ is calculated is reflected in the behaviour observed in these figures. A second point deserving a comment concerns the large uncertainties of our θ_H estimates, in both approaches, which is mainly related to the size of the redshift bin, $z \in [0, 0.3]$. This bin spans a large volume of the universe, and the large

Alonso D., Bueno Belloso A., Sánchez F. J., García-Bellido J., Sánchez E., 2014, MNRAS, 440, 10
 Aluri P. K., Jain P., 2012, MNRAS, 419, 3378
 Appleby S., Shafieloo A., 2014, J. Cosmology Astropart. Phys., 2014, 070
 Asorey J., Carrasco Kind M., Sevilla-Noarbe I., Brunner R. J., Thaler J., 2016, MNRAS, 459, 1293

uncertainties in θ_H indicate that the estimated scale is valid for the diverse epochs of the universe covered by this redshift bin.

Given that our galaxy sample consists of blue galaxies, with a bias $b \simeq 1$, our estimates can be directly compared with the matter homogeneity scale predicted by the Λ CDM model. Therefore, the LS and AFCD observational values are within 0.14σ and 0.28σ , respectively, indicating a consistency between data and theory. Moreover, as shown in Table II, these estimates are also in good agreement with the results obtained with the mock catalogues (analysed following both methodologies).

Tests of homogeneity require a sufficiently wide sky coverage and a suitable number density of cosmic objects, as the transition occurs on large scales. As stated in section II, the analysed S-PLUS region covers 525 deg^2 . While this area already allows a meaningful test of the homogeneity scale in the Local Universe, a natural extension of this work include apply the same methodology to a wider area and, consequently, more populated future data release of S-PLUS. Nevertheless, from the current results, we can already conclude that the blue galaxies sample from the S-PLUS has the potential to validate the CP regarding the angular scale of transition to homogeneity, providing a measurement of such scale, θ_H , in the Local Universe.

ACKNOWLEDGMENTS

CF thanks Coordenação de Aperfeiçoamento de Pessoal de Nível Superior (CAPES) for the financial support. FA thanks to Fundação de Amparo à Pesquisa do Estado do Rio de Janeiro (FAPERJ), Processo SEI-260003/001221/2025, for the financial support. AB acknowledges a CNPq fellowship. This work was carried out using computational resources provided by the Sci-Mind servers machines developed by the CBPF AI LAB team and the Data Processing Center of the National Observatory (CPDON).

DATA AVAILABILITY

The data underlying this article will be shared on reasonable request to the corresponding author.

Avila F., Novaes C. P., Bernui A., de Carvalho E., 2018, J. Cosmology Astropart. Phys., 2018, 041
 Avila F., Novaes C. P., Bernui A., de Carvalho E., Nogueira-Cavalcante J. P., 2019, MNRAS, 488, 1481
 Avila F., Bernui A., Nunes R. C., de Carvalho E., Novaes C. P., 2022, MNRAS, 509, 2994
 Avila F., Oliveira J., Dias M. L. S., Bernui A., 2023, Brazilian

Journal of Physics, 53, 49

Avila F., de Carvalho E., Bernui A., Lima H., Nunes R. C., 2024, MNRAS, 529, 4980

Bagla J. S., Yadav J., Seshadri T. R., 2008, MNRAS, 390, 829

Bamford S. P., et al., 2009, MNRAS, 393, 1324

Bengaly C. A. P., Bernui A., Ferreira I. S., Alcaniz J. S., 2017, MNRAS, 466, 2799

Bernui A., Ferreira I. S., Wuensche C. A., 2008, ApJ, 673, 968

Blot L., et al., 2019, MNRAS, 485, 2806

Bolejko K., Wyithe J. S. B., 2009, J. Cosmology Astropart. Phys., 2009, 020

Chisari N. E., et al., 2019, ApJS, 242, 2

Clarkson C., 2012, Comptes Rendus Physique, 13, 682

Coil A. L., 2013a, in Oswalt T. D., Keel W. C., eds, , Vol. 6, Planets, Stars and Stellar Systems. Volume 6: Extragalactic Astronomy and Cosmology. Springer, p. 387, doi:10.1007/978-94-007-5609-0_8

Coil A. L., 2013b, in Oswalt T. D., Keel W. C., eds, , Vol. 6, Planets, Stars and Stellar Systems. Volume 6: Extragalactic Astronomy and Cosmology. Springer, Dordrecht, p. 387, doi:10.1007/978-94-007-5609-0_8

Colavincenzo M., et al., 2019, MNRAS, 482, 4883

Coleman P. H., Pietronero L., 1992, Phys. Rep., 213, 311

Connolly A. J., et al., 2002, ApJ, 579, 42

Courtois H. M., Pomarède D., Tully R. B., Hoffman Y., Courtois D., 2013, AJ, 146, 69

Courtois H. M., Mould J., Hollinger A. M., Dupuy A., Zhang C. P., 2025, A&A, 701, A187

Crocce M., Cabré A., Gaztañaga E., 2011, MNRAS, 414, 329

Croton D. J., Norberg P., Gaztañaga E., Baugh C. M., 2007, MNRAS, 379, 1562

Dressler A., et al., 1997, ApJ, 490, 577

Einasto M., 1991, MNRAS, 252, 261

Franco C., Avila F., Bernui A., 2024, MNRAS, 527, 7400

Franco C., Oliveira J., Lopes M., Avila F., Bernui A., 2025a, MNRAS, 537, 897

Franco C., Avila F., Bernui A., 2025b, The Astrophysical Journal, 993, 133

Fujii H., 2022, Serbian Astronomical Journal, 204, 29

Galloni G., Bartolo N., Matarrese S., Migliaccio M., Ricciardone A., Vittorio N., 2022, J. Cosmology Astropart. Phys., 2022, 046

Gavas S., Bagla J. S., Khandai N., 2025, Phys. Rev. D, 111, 043516

Gerke B. F., et al., 2007, MNRAS, 376, 1425

Gonçalves R. S., Carvalho G. C., Bengaly Jr. C. A. P., Carvalho J. C., Bernui A., Alcaniz J. S., Maartens R., 2018a, MNRAS, 475, L20

Gonçalves R. S., Carvalho G. C., Bengaly C. A. P., Carvalho J. C., Alcaniz J. S., 2018b, MNRAS, 481, 5270

Gonçalves R. S., Carvalho G. C., Andrade U., Bengaly C. A. P., Carvalho J. C., Alcaniz J., 2021, J. Cosmology Astropart. Phys., 2021, 029

Herpich F. R., et al., 2024, A&A, 689, A249

Huterer D., 2023, A&A Rev., 31, 2

Jarvis M., 2015, TreeCorr: Two-point correlation functions, Astrophysics Source Code Library, record ascl:1508.007

Kester C. E., Bernui A., Hipólito-Ricaldi W. S., 2024, A&A, 683, A176

Khan M. I., Saha R., 2022, J. Cosmology Astropart. Phys., 06, 006

Kurki-Suonio H., 2023, Galaxy Survey Cosmology, <https://www.mv.helsinki.fi/home/hkurkisu/GSC1.pdf>

Landy S. D., Szalay A. S., 1993, apj, 412, 64

Laurent P., et al., 2016, J. Cosmology Astropart. Phys., 2016, 060

Lewis A., Challinor A., 2011, CAMB: Code for Anisotropies in the Microwave Background, Astrophysics Source Code Library, record ascl:1102.026 (ascl:1102.026)

Lippich M., et al., 2019, MNRAS, 482, 1786

Lopes M., Bernui A., Hipólito-Ricaldi W. S., Franco C., Avila F., 2025, A&A, 694, A77

Maartens R., 2011, Philosophical Transactions of the Royal Society of London Series A, 369, 5115

Marques G. A., Bernui A., 2020, J. Cosmology Astropart. Phys., 05, 052

Marques G. A., Novaes C. P., Bernui A., Ferreira I. S., 2018, MNRAS, 473, 165

Mendes de Oliveira C., et al., 2019, MNRAS, 489, 241

Mohammad F. G., et al., 2018, A&A, 610, A59

Novaes C. P., Bernui A., Marques G. A., Ferreira I. S., 2016, MNRAS, 461, 1363

Novaes C. P., et al., 2025, Phys. Rev. D, 111, 083510

Ntelis P., et al., 2017, J. Cosmology Astropart. Phys., 2017, 019

Peebles P. J. E., 1993, Principles of Physical Cosmology. Princeton University Press, doi:10.1515/9780691206721

Pietronero L., 1987, Physica A Statistical Mechanics and its Applications, 144, 257

Planck Collaboration et al., 2020a, A&A, 641, A6

Planck Collaboration et al., 2020b, A&A, 641, A7

Ribeiro U., et al., 2025, arXiv e-prints, p. arXiv:2506.08288

Ross A. J., et al., 2014, MNRAS, 437, 1109

Scrimgeour M. I., et al., 2012, MNRAS, 425, 116

Secrest N. J., von Hausegger S., Rameez M., Mohayaee R., Sarkar S., Colin J., 2021, ApJ, 908, L51

Sylos Labini F., Baryshev Y. V., 2010, J. Cosmology Astropart. Phys., 2010, 021

Telles E., Maddox S., 2000, MNRAS, 311, 307

Tessore N., Loureiro A., Joachimi B., von Wietersheim-Kramsta M., Jeffrey N., 2023, The Open Journal of Astrophysics, 6, 11

Totsuji H., Kihara T., 1969, PASJ, 21, 221

Virtanen P., et al., 2020, Nature Methods, 17, 261

Wu Y.-W., Xia J.-Q., 2025, ApJ, 979, 3

Yadav J. K., Bagla J. S., Khandai N., 2010, MNRAS, 405, 2009

Zehavi I., et al., 2005, ApJ, 630, 1

de Carvalho E., Bernui A., Avila F., Novaes C. P., Nogueira-Cavalcante J. P., 2021, A&A, 649, A20

Řípa J., Shafieloo A., 2019, MNRAS, 486, 3027

Appendix A: Deduction of Equation (12)

The cumulative scaled counts-in-caps within an angular separation θ is defined as

$$\mathcal{N}(< \theta) \equiv 1 + \bar{\omega}(\theta), \quad (A1)$$

where $\bar{\omega}(\theta)$ corresponds to the average angular correlation function, given by

$$\bar{\omega}(\theta) \equiv \frac{1}{1 - \cos \theta} \int_0^\theta \omega(\theta') \sin \theta' d\theta'. \quad (A2)$$

Using these relationships in equation (2), one can derive the expression for the correlation dimension

$$\begin{aligned}\mathcal{D}_2(\theta) &= \frac{d \ln \mathcal{N}(< \theta)}{d \ln \theta} + \frac{\theta \sin \theta}{1 - \cos \theta} \\ &= \frac{\theta}{\mathcal{N}(< \theta)} \frac{d \mathcal{N}(< \theta)}{d \theta} + \frac{\theta \sin \theta}{1 - \cos \theta} \quad (\text{A3}) \\ &= \frac{\theta}{1 + \bar{\omega}(\theta)} \frac{d \bar{\omega}(\theta)}{d \theta} + \frac{\theta \sin \theta}{1 - \cos \theta}.\end{aligned}$$

For convenience, let us introduce the notation

$$I(\theta) \equiv \int_0^\theta \omega(\theta') \sin \theta' d\theta', \quad (\text{A4})$$

then, the derivative of the averaged correlation function can be expressed as

$$\frac{d \bar{\omega}}{d \theta} = \frac{\sin \theta}{(1 - \cos \theta)^2} [\omega(\theta)(1 - \cos \theta) - I(\theta)]. \quad (\text{A5})$$

Finally, substituting this result into equation (A3), the correlation dimension simplifies to

$$\mathcal{D}_2(\theta) = \frac{\theta \sin \theta}{1 - \cos \theta} \left[\frac{1 + \omega(\theta)}{1 + \bar{\omega}(\theta)} \right], \quad (\text{A6})$$

which is the equation (12). This final expression provides a direct relation between the correlation dimension and the TPACF, highlighting how departures from homogeneity can be quantified at a given angular scale.